Partial Oxidation of Propylene to Propylene Oxide over a Neutral Gold Trimer in the Gas Phase: A Density Functional Theory Study

Ajay M. Joshi, W. Nicholas Delgass, and Kendall T. Thomson*

School of Chemical Engineering, Purdue University, West Lafayette, Indiana 47907

Received: August 25, 2005; In Final Form: November 22, 2005

We report a B3LYP study of a novel mechanism for propylene epoxidation using H_2 and O_2 on a neutral Au_3 cluster, including full thermodynamics and pre-exponential factors. A side-on O_2 adsorption on Au_3 is followed by dissociative addition of H_2 across one of the Au—O bonds ($\Delta E_{act} = 2.2$ kcal/mol), forming a hydroperoxy intermediate (OOH) and a lone H atom situated on the Au_3 cluster. The more electrophilic O atom (proximal to the Au) of the Au—OOH group attacks the C═C of an approaching propylene to form propylene oxide (PO) with an activation barrier of 19.6 kcal/mol. We predict the PO desorption energy from the Au_3 cluster with residual OH and H to be 11.5 kcal/mol. The catalytic cycle can be closed in two different ways. In the first subpathway, OH and H, hosted by the same terminal Au atom, combine to form water ($\Delta E_{act} = 26.5$ kcal/mol). We attribute rather a high activation barrier of this step to the breaking of the partial bond between the H atom and the central Au atom in the transition state. Upon water desorption ($\Delta E_{des} = 9.9$ kcal/mol), the Au_3 is regenerated (closure). In the second subpathway, H_2 is added across the Au—OH bond to form water and another Au—H bond ($\Delta E_{act} = 22.6$ kcal/mol). Water spontaneously desorbs to form an obtuse angle Au_3 dihydride, with one H atom on the terminal Au atom and the other bridging the same terminal Au atom and the central Au atom. A slightly activated rearrangement to a symmetric triangular Au_3 intermediate with two equivalent Au—H bonds, addition of O_2 into the Au—H bond, and rotation reforms the hydroperoxy intermediate in the main cycle. On the basis of the ΔG_{act}, which contains contribution from both pre-exponetial factor and activation energy, we identify the propylene epoxidation step as the actual rate-determining step (RDS) in both the pathways. The activation barrier of the RDS (epoxidation step: $\Delta E_{act} = 19.6$ kcal/mol) is in the same range as that in the published computationally investigated olefin epoxidation mechanisms involving Ti sites (without Au involved) indicating that isolated Au clusters and possibly Au clusters on non-Ti supports can be active for gas-phase partial oxidation, even though cooperative mechanisms involving Au clusters/Ti-based-supports may be favored.

1. Introduction

A series of pioneering results published by Haruta and coworkers[1,2] has stimulated a global activity in the field of catalysis by gold. These worldwide efforts are responsible for significant advances in understanding the catalytic activity of Au nanoparticles. It is interesting to note that Au, which is noble in the bulk state,[3] when employed in the form of supported nanoparticles, can in fact catalyze a variety of chemical reactions, for example, CO oxidation[4−6] and propylene partial oxidation to propylene oxide (PO).[7−12] Various kinds of surface defects are found to be responsible in "making gold less noble".[13] Highly dispersed nanometer-sized supported Au particles have shown remarkable catalytic activity in CO oxidation.[4,5] Au nanoparticles supported on TiO_2,[7,8,12] TS-1,[11,14] Ti−MCM-41,[9] and Ti−MCM-48[10] are active in the gas-phase partial oxidation of propylene to PO using H_2 and O_2. It is claimed that the cluster-support interaction plays an important role in the activity of supported Au catalysts.[13,15,16] In the case of the Au/TS-1 catalyst, nanometer-sized Au particles must reside on the external surface of the TS-1. However, there is indirect experimental evidence suggesting that the small Au ensembles residing inside the TS-1 channels may also be active in propylene epoxidation.[14] In the liquid-phase epoxidation using TS-1, hydrogen peroxide is used as an oxidizing agent, which converts the propylene to PO at the active Ti site.[17−19] In the gas-phase epoxidation process, Au/TS-1 and other Au/Ti catalysts oxidize the propylene using H_2 and O_2. Therefore, it is reasonable to postulate that Au plays some role in the in situ formation of either hydrogen peroxide or some other oxidizing agent(s), which then carry out the propylene oxidation. One possibility is the exact analogue of the liquid-phase epoxidation process, i.e., Ti plays a direct role in the epoxidation of propylene using the oxidizing agent(s) formed on the active Au. Another possibility is that the Ti is playing an indirect role in the catalytic reaction by simply activating the Au clusters anchored in its vicinity. In that case, both the formation of the oxidizing agent(s) as well as the propylene epoxidation may occur on the small Au clusters, assigning a dual role to Au. It is also possible that both the pathways coexist and that the pathway with a direct role of Ti in the epoxidation dominates, due to a lower activation barrier. For these reasons and to fully understand the potential reactivity of Au clusters, there is a need to investigate PO formation mechanisms occurring entirely on the Au clusters. We believe that such a pathway is important not only in the context of nanogold supported on Ti-containing supports but also in the context of non-Ti-containing supports. A first step toward exploring this possibility involves experimental and computa-

* To whom correspondence should be addressed. Email: thomsonk@ecn.purdue.edu. Phone: (765) 496-6706. Fax: (765) 494-0805.

10.1021/jp054809f CCC: $33.50
Published on Web 01/26/2006

tional investigations of the activation of propylene, H_2, and O_2 by Au nanoclusters.

A temperature-programmed desorption (TPD) study by Ajo et al.[20] suggests that propylene is adsorbed at the Au−TiO_2-(110) interface and on the one-atom-thick Au islands. A recent inelastic neutron scattering (INS) study by Goodman and co-workers[21] offers (for the first time) experimental evidence for the reaction of H_2 and O_2 to form hydrogen peroxide and hydroperoxy (OOH) kind of species on the Au/TiO_2 catalyst. Goodman and co-workers[22] also studied the adsorption of propylene on clean and oxygen-covered Au(111) and Au(100) surfaces. Small amounts of products (most probably PO) with masses 56 and 58 amu were observed during the TPD of propylene adsorbed onto a 0.4 ML oxygen-covered surface; these products, of course, formed due to the interaction between propylene and oxygen (no H_2 was present) on Au surfaces. It must be noted that Au nanoparticles are expected to be much more active than the extended Au surfaces. Also, the hydroperoxy (OOH) species formed from the H_2 and O_2 are expected to be more active for the oxidation reactions compared to O_2. Therefore, there is a possibility of a PO formation pathway occurring exclusively on small Au clusters, with only an indirect role of the support.

Nijhuis et al.[12] reported on the possibility of the Au clusters playing a larger role than merely acting to produce the oxidizing agent and proposed a bidentate propoxy species on the Au/TiO_2 catalyst as a reaction intermediate in the propylene oxidation pathway. Their experimental data for the Au/TiO_2 catalyst implies that propylene is adsorbed on Au. For the closely related system of CO oxidation on rutile-supported Au clusters, a recent density functional theory (DFT) study by Remediakis et al.[23] illustrates a CO oxidation mechanism occurring exclusively on Au. In a series of publications, Chrétien et al.[24−26] have reported computational analysis of propylene adsorption on small Au, Ag, and mixed Au−Ag clusters (with only a few noble metal atoms) in the gas phase. They succeeded in identifying the propensity rules for the propylene binding on these noble metal clusters. A previous publication from our group[27] reported a gas-phase hydrogen peroxide formation pathway on the neutral Au trimer. A hydroperoxy (OOH) intermediate was identified to be the precursor for the full closed-loop catalytic cycle. This computational study is substantiated by the experimental observation of hydroperoxy and hydrogen peroxide species by Goodman and co-workers.[21] Thus, both theory and experiment support hydroperoxy (OOH) formation on Au clusters. A natural continuation of our previous work is to study the formation of PO from propylene, H_2, and O_2. Considering our experience, neutral Au_3 is the best candidate to start the computational study of propylene epoxidation on Au alone.

In this paper, we report a DFT investigation of the propylene epoxidation on the neutral Au_3 cluster using H_2 and O_2. We used the B3LYP density-functional and 6-311+G(3df) basis set for the C, O, and H. A relativistic pseudopotential LANL2DZ (and the corresponding double-ζ basis set) was employed to describe Au. We report two closely related pathways for the propylene epoxidation. The main reactions in our catalytic cycles are: (i) formation of the hydroperoxy (OOH) intermediate from O_2 and H_2 on Au_3, (ii) attack of propylene on the (more electrophilic) O atom proximal to the Au atom in the hydroperoxy intermediate to form PO, and (iii) water formation leading to the closure of the catalytic cycle. The two pathways differ in the way the catalytic cycle is closed. We also report a detailed thermochemistry along with pre-exponential factors for the important steps and Natural Bond Orbital (NBO) charge analysis of the various intermediates and transition states in the pathway.

TABLE 1: A Comparison of the Calculated and Experimental Properties[a]

molecule	predicted EA (kcal/mol)	experimental EA (kcal/mol)	predicted IP (kcal/mol)	experimental IP (kcal/mol)
Au_1	49.95	51.82 [37]	217.26	212.58[38]
Au_2	46.77	46.52 [37]	224.13	210.97[39]
Au_3	84.87	86.83 [37]	167.49	167.44[39]
Au_4	64.92	63.80 [37]	184.86	198.07[40]
Au_5	73.28	71.86 [37]	165.07	175.27[39]
O_2	11.31	10.36 [43]	289.60	277.77[44]
propene			219.90	223.47[45]
PO			233.55	236.62[46]

[a] References for the experimental data are indicated as a superscript of the value.

2. Computational Method

Our electronic DFT calculations were conducted using the Gaussian 03 suite of programs.[28] We used the 1993 three-parameter hybrid functional of Becke (B3LYP).[29] In B3LYP, the exchange term is described by the exchange functional of Becke, the nonlocal correlation is described by the LYP expression,[30] and the local correlation is described by the VWN III functional.[31] We used the Los Alamos LANL2DZ[32,33] effective core pseudopotential (ECP) and corresponding valence double-ζ basis set for Au, and the 6-311+G(3df) basis set for carbon, oxygen, and hydrogen. In what follows, we briefly discuss the rationale behind our choice of the DFT functional, pseudopotential, and basis set.

Since Au atom has seventy-nine electrons, calculations including all electrons were out of consideration, and the obvious choice was to use an effective core pseudopotential. The LANL2DZ pseudopotential was chosen particularly because of the advantage of doing faster calculations with relatively little compromise on accuracy. Literature reports on Au have emphasized strong relativistic effects,[34−36] and the LANL2DZ pseudopotential accounts for these effects. To further support our choice of the DFT functional and the pseudopotential, we provide benchmark calculations in the Table 1. All the predicted values are in agreement with the corresponding experimental values.[37−40] It is well known that the prediction of the electron affinity of oxygen is a challenging task.[41,42] One needs to add diffuse functions in the basis set to predict the oxygen electron affinity accurately. Also, a relatively large basis set can improve the accuracy of the reaction energetics, i.e., adsorption and activation energies. Therefore, we chose a 6-311+G(3df) (triple-ζ) basis set with diffuse and polarization functions for carbon, oxygen, and hydrogen atoms. Again, it is clear from the Table 1 that B3LYP/6-311+G(3df) provides accurate predictions of the properties of the relevant molecules.[43−46]

Although electron affinity (EA) predictions are excellent, ionization potential (IP) predictions are not as good. Therefore, some remarks about interpreting the accuracy of our calculations are in order. We first point out that IP of Au_3 is in excellent agreement with the experimental value and hence the set of calculations used to find energetics reported in this paper probably have minimal errors. However, in the case of other Au clusters IP predictions are apparently not as good. To address this issue we performed very time intensive state-of-the-art coupled-cluster CCSD(T) calculations with a relatively much better basis set (cc-PVTZ-PP). Because of computer time limitations, we only predicted an IP value of Au_1; the predicted value (206.00 kcal/mol) is 6.58 kcal/mol lower than the

experimental value. The predicted value using b3lyp/lanl2dz is 217.26 kcal/mol, 4.68 kcal/mol higher than the experimental value. We point out that the Au atoms involved in our reaction mechanism do not carry a full positive charge on them and hence the errors in predicting IP values can be treated as the maximum possible errors and should not be treated as the absolute errors in the energetics of our reaction mechanisms. Therefore, we conclude that the errors in the DFT scheme reported in this paper are likely to be much lower than they appear to be from the IP predictions. Even CCSD(T) calculations with the cc-PVTZ-PP basis set do not give better predictions of the IP of Au_1. Improved IP predictions could be obtained by employing valence-correlated and core-valence complete basis set (CBS) limits. However, noting the extremely large computer time involved, it is impractical to use such an advanced level of theory to unravel reaction pathways.

In all the adsorption and reaction steps, we considered several different orientations or starting geometries and carried out full geometry optimization at the aforementioned level of theory. We considered both in-plane as well as out-of-plane attacks, and investigated many combinations of distances, angles, and solid angles. Thus, we generated an ensemble of different geometries and selected the lowest-energy state, i.e., the ground state, to represent the reaction intermediates in our reaction pathway and hence the thermodynamics and kinetics of the reaction. Throughout the paper, we report the binding energies (BEs) calculated as: BE = E(reactants) − E(products), i.e., $\Delta E = -\mathrm{BE}$. Here E is the electronic energy calculated at 0 K in a vacuum. Therefore a positive binding energy means negative ΔE, i.e., exothermic reaction/adsorption step. In the text, we use ΔE_{act} to denote the electronic energy of activation and ΔE_{des} to denote the electronic energy of desorption, both calculated at 0 K in a vacuum. Similar notation is used for other thermodynamic quantities such as Gibbs free energy (G), i.e., if the change in the Gibbs free energy (ΔG) is negative then the adsorption is thermodynamically favorable.

The frequency calculations were performed on all the intermediates and transition states. In case of the stable intermediates, we verified that all the frequencies are positive, and in case of the transition states, we verified that there is only one imaginary frequency. These frequency calculations also provided us with the thermochemical analysis at a pressure of 1 atm and a temperature of 298.15 K. We report the change in the Gibbs free energy (ΔG at standard conditions) and pre-exponential factors for the important steps. The pre-exponential factors were calculated using the molecular partition functions as

$$A_{\mathrm{uni}} = \frac{k_{\mathrm{B}}T}{h}\frac{Q_{\mathrm{TS}\dagger}}{Q_{\mathrm{A}}}$$

$$A_{\mathrm{bi}} = \frac{k_{\mathrm{B}}T}{h}\frac{Q_{\mathrm{TS}\dagger}}{Q_{\mathrm{A}}Q_{\mathrm{B}}}$$

where A_{uni} and A_{bi} are the pre-exponential factors (for unimolecular and bimolecular reactions, respectively), k_{B} is Boltzmann's constant, h is Planck's constant, T is absolute temperature, Q_{A} and Q_{B} are the partition functions per volume of reactant molecules A and B, and $Q_{\mathrm{TS}\dagger}$ is the partition function per volume of the transition state, excluding the vibrational mode corresponding to the reaction coordinate. In the case of bimolecular reactions, the units of the pre-exponential factors (see Tables 2 and 3) are implicitly reported as m^3/s. However, we point out that the explicit units are m^3/molecule-s, i.e., in calculating the rates, the concentration terms should be in molecules/m^3 (/m^3 in implicit form). We also calculated the rate constants at standard conditions using the pre-exponential factor and zero-point-corrected activation energy. Natural Bond Orbital (NBO)[47] analysis of the electron population on each atomic center was performed using the Gaussian 03 suite.[28] Annihilation of spin contaminants was carried out by default in Gaussian 03.[28]

TABLE 2: Summary of the Energetics of the PO Formation Pathway on the Au_3[a]

reaction step	ΔE[b] (kcal/mol)	ΔE_{zpe}[c] (kcal/mol)	ΔU[d] (kcal/mol)	ΔG[e] (kcal/mol)	pre-exponential factor
A + O_2 → B	−7.00	−6.17	−5.83	4.64	
B + H_2 → C-TS	2.18	4.33	3.22	11.29	2.02×10^{-18} m^3/s
B + H_2 → D	−17.99	−13.12	−13.85	−6.83	
D + C_3H_6 → F-TS	19.58	20.52	20.76	32.17	7.28×10^{-22} m^3/s
D + C_3H_6 → G	−51.38	−48.61	−48.23	−38.85	
G → H + PO	11.48	10.57	9.42	0.84	
H → I-TS	26.55	25.39	25.53	25.03	1.13×10^{13} /s
H → J	−25.96	−23.18	−22.65	−24.43	
J → water + A	9.87	7.97	7.62	−0.10	

[a] The symbols A, B, etc., correspond to the geometries described in Figures 1−5. Here we have included only the first subpathway (last three steps). [b] The difference in the electronic energies of the products and the reactants at 0 K. [c] The difference in the electronic energies of the products and the reactants at 0 K with proper accounting of the zero-point energy. [d] The difference in the internal energies of the products and the reactants at 298 K and 1 atm pressure. [e] The difference in the Gibbs free energies of the products and the reactants at 298 K and 1 atm pressure. Note: If the reaction step in the table involves a transition state on the product side, then the ΔE corresponds to the ΔE_{act}. Similar considerations apply to other thermodynamic quantities.

TABLE 3: Summary of the Energetics of the PO Formation Pathway on the Au_3[a]

reaction step	ΔE[b] (kcal/mol)	ΔE_{zpe}[c] (kcal/mol)	ΔU[d] (kcal/mol)	ΔG[e] (kcal/mol)	pre-exponential factor
H + H_2 → K-TS	22.58	23.74	22.81	30.39	3.36×10^{-18} m^3/s
H + H_2 → L	−8.59	−4.22	−4.39	0.75	
L → M + water	−1.77	−4.30	−4.38	−12.12	
M → N-TS	3.84	3.66	3.06	4.81	8.96×10^{11}/s
M → O	−5.37	−4.65	−4.89	−3.74	
O + O_2 → P	−25.01	−20.91	−20.58	−11.24	
P → Q-TS	4.44	3.66	3.58	3.44	9.06×10^{12}/s
P → R or D	−0.32	−0.41	−0.47	−0.37	

[a] The symbols A, B, etc., correspond to the geometries described in Figures 1−5. Here we have included the second subpathway. The first six steps (not shown) are the same as those in Table 2. [b] The difference in the electronic energies of the products and the reactants at 0 K. [c] The difference in the electronic energies of the products and the reactants at 0 K with proper accounting of the zero-point energy. [d] The difference in the internal energies of the products and the reactants at 298 K and 1 atm pressure. [e] The difference in the Gibbs free energies of the products and the reactants at 298 K and 1 atm pressure. Note: If the reaction step in the table involves a transition state on the product side, then the ΔE corresponds to the ΔE_{act}. Similar considerations apply to other thermodynamic quantities.

In what follows, we discuss in detail the PO formation over the neutral Au trimer in the gas phase. All the geometries identified by the letters A, B, etc. (names reported in brackets in the text), are reported in Figures 1−5, and reaction energetics are presented in Figures 6 and 7. Tables 2 and 3 contain the thermochemistry details, while Table 4 contains the NBO charge details of all the geometries in the catalytic cycles.

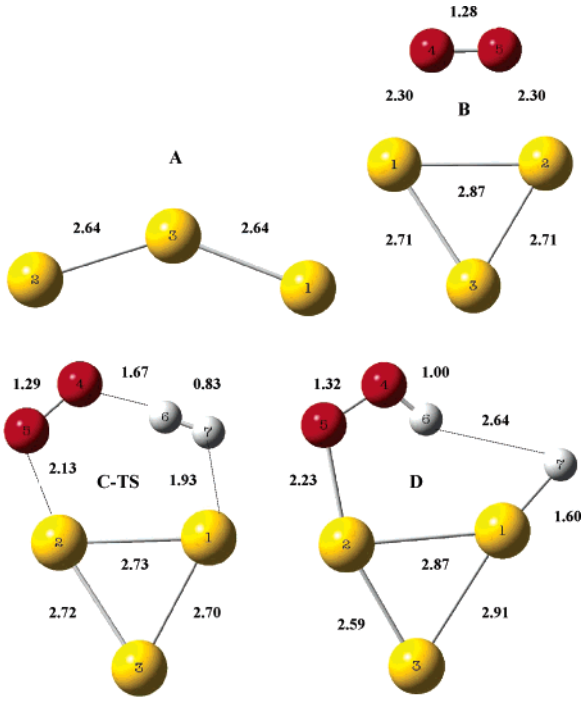

Figure 1. Geometries of various species involved in the OOH formation on the Au_3. Distances are in angstroms. The rest of the details of these geometries and the geometries in the subsequent figures are available from authors upon request.

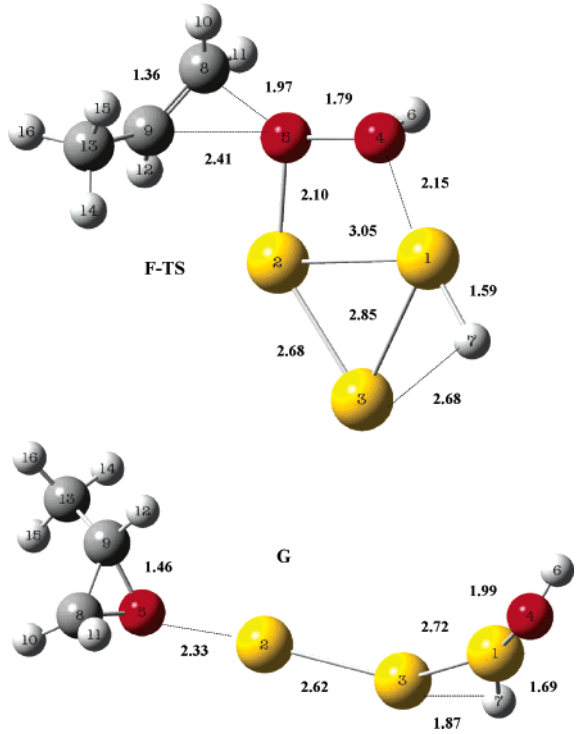

Figure 2. Geometries of the transition state and product in the propylene oxidation step. Distances are in angstroms.

3. Results

3.1. Formation of the Hydroperoxy (OOH) Precursor on Au_3. A BPW91 (DFT) study of the formation of hydrogen peroxide on the neutral Au_3 was recently reported by Wells et al.[27] In fact, we have also investigated full catalytic cycles for hydrogen peroxide formation on gas-phase Au_3, Au_4^+, Au_5, and Au_5^-, all at the same level of theory as that used in this work.[48] A hydroperoxy intermediate formed on the Au cluster was found

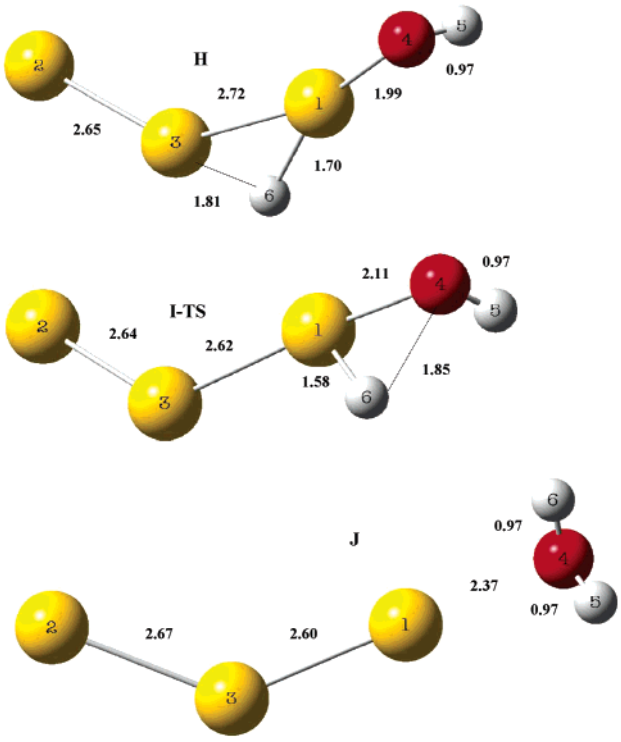

Figure 3. Geometries of various species involved in the subpathway 1. Distances are in angstroms.

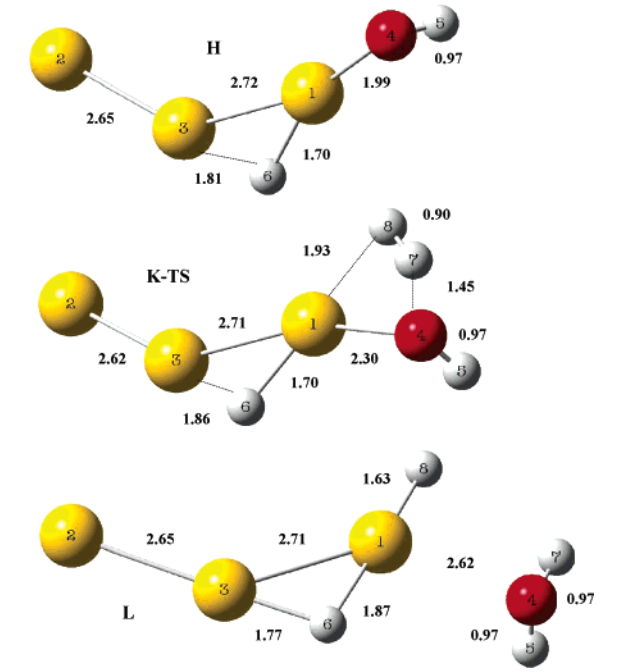

Figure 4. Geometries of various species involved in the H_2 addition step of subpathway 2. Distances are in angstroms.

to be the precursor of the catalytic cycle. To achieve completeness and continuity in this paper, we briefly discuss this chemistry on Au_3. All the relevant geometries are reported in the Figure 1.

We tried several different starting geometries and carried out full geometry optimizations to obtain the ground state of Au_3. In agreement with both computational[35,49] and experimental studies,[50] we found this geometry (A) to be an obtuse angle (140.9°) triangle (asymmetry due to the Jahn−Teller distortions). Attack on this Au_3 geometry (A) by O_2 was then examined. Both doublet and quartet spin states for the O_2 adsorbed on the

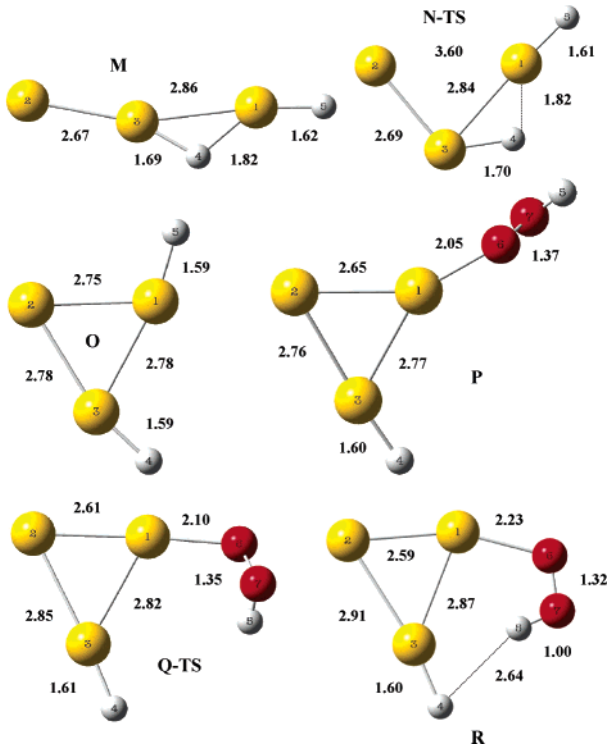

Figure 5. Geometries of various species involved in the closure part of subpathway 2. Distances are in angstroms.

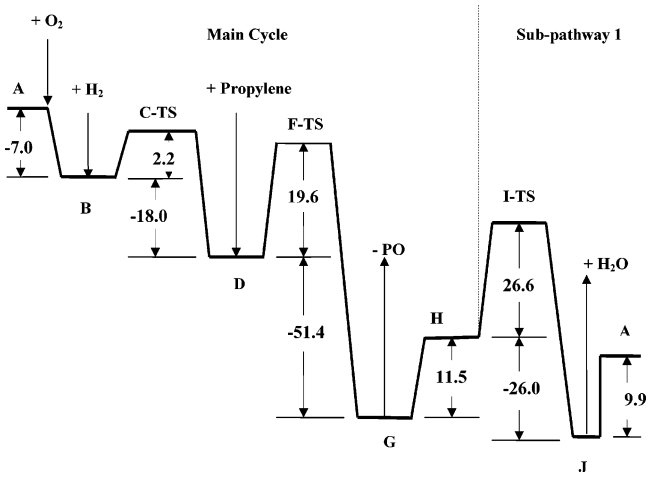

Figure 6. A schematic of the energetics of the PO formation pathway on the Au_3. This figure represents the main catalytic cycle and the subpathway 1. The differences in the electronic energies at 0 K are indicated for each step.

Au_3 were investigated, as required because the ground state of the O_2 molecule is a triplet. Again, in agreement with the literature,[51,52] we found a doublet ground state, which is a planar geometry (B) with side-on bound O_2. It should also be noted that there is a significant reduction in the obtuse angle of the Au_3 upon O_2 adsorption (63.8°, almost an equilateral triangle). NBO analysis indicates that there is almost −0.50 charge on the adsorbed O_2 (i.e., almost +0.50 charge on Au_3 indicating an oxidic Au species), which is an evidence for the charge transfer from the Au_3 to the O_2. As expected, a corresponding elongation in the O−O bond length from a gas-phase value of 1.20 Å to a value of 1.28 Å in the adsorbed state is also observed. The binding energy of the side-on bound O_2 on Au_3 to is 7.0 kcal/mol ($\Delta E = -7.0$ kcal/mol).

A very specific mechanism for the hydrogen attack on this Au_3O_2 species exists, in which H_2 dissociates and forms a OOH

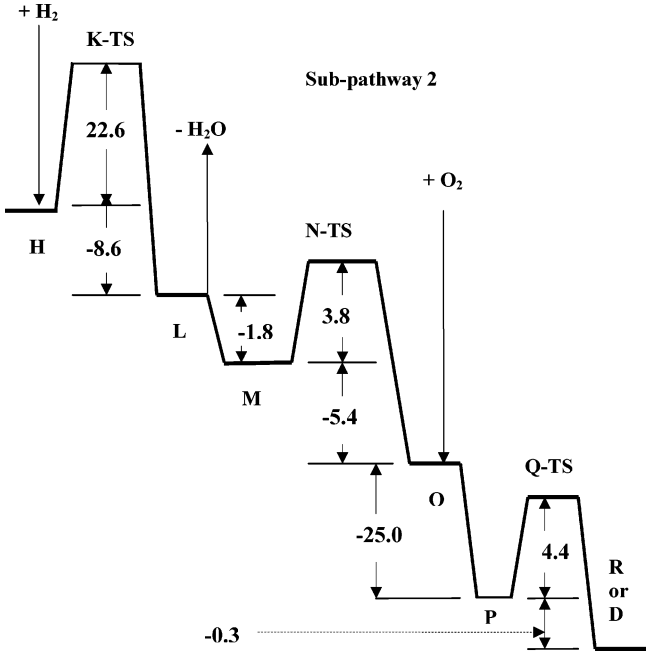

Figure 7. A schematic of the energetics of the PO formation pathway on the Au_3. This figure represents the sub-pathway 2 (starting from the geometry H). The differences in the electronic energies at 0 K are indicated for each step.

TABLE 4: NBO Charge Analysis of Various Species Involved in the PO Formation on Au_3 [a]

atom no./ species	1	2	3	4	5	6	7	8
A	0.036	−0.072	0.036					
B	0.301	0.299	−0.108	−0.247	−0.245			
C-TS	0.330	0.395	−0.181	−0.230	−0.311	0.172	−0.175	
D	0.030	0.274	−0.119	−0.260	−0.202	0.484	−0.207	
H	0.606	0.014	0.107	−0.926	0.450	−0.251		
I-TS	0.482	−0.021	−0.121	−0.939	0.448	0.151		
J	0.102	−0.055	−0.118	−0.911	0.491	0.491		
K-TS	0.606	−0.054	0.074	−0.893	0.454	−0.248	0.204	−0.143
L	0.454	−0.082	0.180	−0.897	0.478	−0.371	0.483	−0.245
M	0.234	0.029	0.054	−0.180	−0.137			
N-TS	0.176	0.011	0.172	−0.172	−0.187			
O	0.220	−0.024	0.059	−0.133	−0.122			
P	0.475	−0.149	0.093	−0.179	0.467	−0.359	−0.348	
Q-TS	0.422	−0.137	0.088	−0.215	0.470	−0.329	−0.299	
F-TS	0.414	0.394	0.000	−0.754	−0.606	0.467	−0.186	−0.249
G	0.594	0.110	0.037	−0.990	−0.600	0.446	−0.270	−0.047

atom no./ species	9	10	11	12	13	14	15	16
F-TS	−0.121	0.204	0.204	0.201	−0.610	0.216	0.210	0.216
G	0.092	0.187	0.193	0.198	−0.591	0.215	0.210	0.216

[a] The atom numbers are indicated in Figures 1−5. The nomenclature A, B, etc., is the same as that followed in Figures 1−5 and the text.

intermediate connected to the Au atom no. 2 (D), while the second H atom attaches to the Au atom no. 1. The activation energy (ΔE_{act}) for this H_2 addition is only 2.2 kcal/mol (see Table 2). This is in agreement with BPW91 study by Wells et al.[27] who reported almost barrierless formation of the hydroperoxy intermediate. They also carried out constrained optimizations to verify the negligible activation barrier.[27] In reference to the present study, the H−H distance increases substantially from 0.835 Å in the transition state (C-TS) to 2.637 Å in the product (D). It may appear that the barrier for this step is too low to cause such a significant change in the geometry. However, we point out that the product geometry was rigorously verified by using many points in intrinsic reaction coordinate

(IRC) calculations. Also, the H−H bond length of isolated gas-phase H_2 is 0.743 Å, which increases only by 0.1 Å in the transition state, consistent with the low activation energy (2.2 kcal/mol).

It is interesting to note that in the transition state (C-TS) for the H_2 addition, the net NBO charge on the Au_3 is +0.54, which reduces to +0.19 after the hydroperoxy intermediate (D) is formed. In the hydroperoxy intermediate (D), the net NBO charge on the O_2 in the OOH group is −0.46, which is slightly less negative and thus more electrophilic than the −0.50 charge on the adsorbed O_2. It should also be noted that the proximal O atom (no. 5 attached to Au atom no. 2 in geometry D) of the OOH is more electrophilic (NBO charge −0.20) than the distal O atom no. 4 (NBO charge −0.26). The H_2 addition step to form the hydroperoxy intermediate is exothermic with the $\Delta E = -18.0$ kcal/mol and $\Delta G = -6.8$ kcal/mol indicating a thermodynamically favorable formation of the hydroperoxy intermediate.

3.2. Propylene Attack on the OOH Precursor to Form PO. All the relevant geometries for this discussion are reported in Figures 2 and 3. The reaction of propylene to form PO has an activation energy of 19.6 kcal/mol. NBO charge analysis of the transition state (F-TS) of this step clearly indicates that propylene loses significant electron density to the OOH group. The NBO charge on the proximal O atom (no. 5) in the transition state (F-TS) is −0.60, which is substantially more negative than its −0.20 charge in the hydroperoxy intermediate (D). We note that the more electrophilic proximal (to the Au atom) O atom (no. 5) of the OOH group (D) attacks the double bond of the propylene to form PO. This observation is consistent with the DFT study of the propylene oxidation on the defect Ti site of the TS-1, which demonstrates the attack of the electrophilic O atom of the Ti−OOH on the propylene.[53]

It is interesting to note that during the oxidation step, the residual hydroxyl (OH) group of the hydroperoxy species (D) moves closer to the Au atom (no. 1) having one H atom (no. 7) already attached to it. H atom no. 7 rotates to create more space for the invasive OH group (G). This means that both the H atom no. 7 and the OH (terminal part of the OOH) species are anchored to the same Au atom as depicted in the geometry G. This motion is described by the NBO charges in the transition state (F-TS); the distant O atom (no. 4, of the OH) has −0.75 charge on it and hence approaches a more positively charged Au atom (no. 1). The Au atom (no. 2), which previously hosted the OOH has +0.39 charge on it, while the Au atom (no. 1), which has one H atom attached to it, has +0.41 charge on it (F-TS). Therefore, the residual OH group attacks this latter Au atom (no. 1). Also, the steric factors (shorter distance) make the attack on Au atom no. 1 more favorable.

The reaction path from the transition state (F-TS) to the product state (G) is also very interesting. Because of the positive charges on the two Au atoms (no. 1 and no. 2), Coulombic repulsive forces open up the Au_3 to form an obtuse angle (135.6°) triangle. In this product state (G), PO remains adsorbed on the Au atom (no. 2), which donated the proximal O atom to the propylene. This Au atom (no. 2) in the product state (G) has +0.11 charge and hence interacts with the O atom (NBO charge of −0.60) of the PO. As mentioned earlier, the other terminal Au atom (no. 1) is connected to both the OH and H species. H atom no. 7 actually bridges the terminal Au atom (no. 1) and the central Au atom (no. 3), which had been just a spectator up to this point. Such coordination also helps in reducing the crowding on Au atom no. 1.

The PO formation step is highly exothermic and has ΔE of −51.3 kcal/mol and ΔG of −38.9 kcal/mol. Desorption of PO requires 11.5 kcal/mol (ΔE_{des}), while the corresponding ΔG_{des} is only 0.8 kcal/mol. The obtuse angle Au_3 species formed after the PO desorption has negatively charged OH and H groups connected to the same Au atom (Figure 3, geometry H). To reduce the Coulomb repulsion, the OH and H groups are located quite far from each other. Starting from this geometry, we discovered two different pathways leading to the closure of the catalytic cycle.

3.3.1. Subpathway I for the Closure of the Catalytic Cycle. All the relevant geometries for this discussion are depicted in the Figure 3. The reaction stoichiometry dictates that, for every PO molecule, one water molecule must form. One way to guarantee this requirement is the combination of OH and H groups on Au atom no. 1 to form water. We analyzed this pathway and the resultant product water adsorbed on the Au_3 is shown in the geometry (J). We also report the transition state (I-TS) for this transformation. While moving from the reactant state (H) to the transition state (I-TS), the H atom (no. 6), which was coordinated to the two Au atoms, moved away from the central Au atom (no. 3), and came closer to the OH group.

It is interesting to note that this H atom (no. 6) in the reactant state (H) has −0.25 NBO charge, while in the transition state it has +0.15 NBO charge; the NBO charge on the O atom (no. 4) and the H atom (no. 5) of the OH group remained almost the same as that in the reactant state (H). This means that H atom no. 6 started behaving more like a H atom in the water molecule, since the H atoms in the water molecule are positively charged. Also, the reaction coordinate involves just the rotation of the H atom (no. 6) toward the OH group. However, this step has a high activation barrier ($\Delta E_{act} = 26.5$ kcal/mol, $\Delta G_{act} = 25.0$ kcal/mol), and based only on the ΔE_{act} it appears to be the rate-determining step (RDS) of the whole catalytic cycle (with subpathway 1). This barrier is high due to the fact that the H atom (no. 6) coordinating with two Au atoms (nos. 1 and 3) was stabilized due to the hydridelike nature of the interaction in the reactant (H), and this stability was lost in the transition state (I-TS). The activation energy is, therefore, almost the energy needed to break the partial hydridelike bond formed between the central Au atom (no. 3) and the H atom (no. 6). However, the water formation step is highly exothermic ($\Delta E = -25.9$ kcal/mol) and hence thermodynamically favorable ($\Delta G = -24.4$ kcal/mol). About 9.9 kcal/mol energy is needed to desorb the water molecule. In fact, the ΔG_{des} is slightly negative (−0.1 kcal/mol), indicating a spontaneous desorption and this step results into the regeneration of the obtuse angle Au_3 cluster (closure of the cycle).

3.3.2. Subpathway II for the Closure of the Catalytic Cycle. We stated in the subpathway I that the activation barrier for the water formation is quite high due to the breaking of the partial bond between the Au atom and the H atom in the transition state. We thought that the activation barrier could be lowered if this transformation could be carried out through a transition state that did not involve any "net" bond breaking. We now discuss this alternative pathway for the closure of the catalytic cycle. All the relevant geometries are shown in Figures 4 and 5.

Again, the starting point (Figure 4, geometry H) is an Au_3 species with OH group and H atom attached to the same terminal Au atom (no. 1), and the H atom (no. 6) also coordinating with the central Au atom (no. 3). We considered the dissociative addition of H_2 across the Au−OH bond to generate the water molecule and another Au−H bond. Indeed, we found that the

activation barrier for this H_2 addition ($\Delta E_{act} = 22.6$ kcal/mol) is lower than the activation barrier for the water formation in the first subpathway. However, the ΔG_{act} is 30.4 kcal/mol, which is higher than the 25.0 kcal/mol in the first sub pathway. In the transition state (K-TS) for the dissociative H_2 addition, the H atom (no. 7, of the H_2) attacking the O atom (no. 4) of the OH group has +0.20 NBO charge (waterlike behavior), while the other H atom (no. 8, of the H_2), which attacks the Au atom (no. 1), has −0.14 NBO charge (hydridelike behavior).

The product state (L) involves a water molecule adsorbed on the Au_3 species, which now hosts two hydridelike hydrogen atoms. Although the ΔE for this H_2 addition step is −8.6 kcal/mol, the *standard* ΔG is actually slightly positive (0.8 kcal/mol). Surprisingly, water desorption is spontaneous: $\Delta E_{des} = -1.8$ kcal/mol and $\Delta G_{des} = -12.1$ kcal/mol. This may be due to the high stability of the product (see geometry M) dihydride of the Au_3, which involves one H atom (no. 5, which came from the new H_2) bonded to the terminal Au atom (no. 1) and another H atom (no. 4) partially bonded to both the terminal Au atom (no. 1) and central Au atom (no. 3). The NBO charges on these H atoms are −0.14 (no. 5) and −0.18 (no. 4), respectively (see geometry M). It is interesting to note that the Au_3 cluster is almost linear in this state (M), with obtuse angle $\approx 162°$. This hydridelike geometry is different than the one we found in the hydrogen peroxide formation pathway on the Au_3,[48] which was also hydridelike but had a configuration close to an equilateral triangle.

We identified a small activation barrier (3.8 kcal/mol) to move from the almost linear Au_3 hydride (M), through the transition state N-TS, to the Au_3 hydride species (O), similar to that reported by us in hydrogen peroxide formation pathway.[48] In fact, we found that this more symmetric hydride (O) is about 5.4 kcal/mol lower in energy than the geometry M. We want to point out that in the symmetric hydride species (O) there is one H atom (no. 4) bonded to the Au atom (no. 3), which previously was the central Au atom in the obtuse-angle geometry. Therefore, the central Au atom (no. 3), which was just a spectator in most of the steps, is now bonded to the H atom (no. 4).

The next steps of the reaction are exactly the same as those reported by Wells et al.[27] and the current authors[48] in the peroxide formation pathway. There is apparently an unactivated addition of the O_2 in to the Au−H bond (of the Au atom no. 1) to form the hydroperoxy species (P). Despite several attempts using rigorous searches involving quasi-Newton and other algorithms to locate a transition state for this transformation, we could not locate any. This issue was addressed further in the previous publication from our group.[27] A series of optimizations involving a constraint on the distance between the H atom of the Au−H bond and the O atom of the attacking O_2 were carried out by varying this constrained distance and allowing all other degrees of freedom to relax completely.[27] Such a methodology can provide a rough estimate of the reaction path. An existence of a maximum in the energy with respect to the change in the constrained H−O distance would indicate existence of the activation barrier for the attack of O_2 and would actually provide an upper bound on the activation energy. However, no maximum was found, and hence it is likely that the attack of O_2 on Au−H is unactivated.[27] Nevertheless, we acknowledge that there may be a transition state in this transformation that we failed to locate. If such a transition state exists then we expect that it would have a lower activation barrier than that in other kinetically important steps, due to a stronger O−H bond than Au−H bond, as implied by the high exothermicity of this O_2 addition step ($\Delta E = -25.0$ kcal/mol).

This O_2 addition step is, in fact, spontaneous at room temperature with $\Delta G = -11.2$ kcal/mol. However, the hydroperoxy geometry formed (P) is slightly different than the one formed at the beginning of the main cycle (Figure 1, geometry D). There is a 4.5 kcal/mol activation barrier for the rotation of the hydroperoxy geometry (P), through the transition state Q-TS, to the geometry (R) similar to the one formed at the beginning of the main catalytic cycle (D). The rotation step results in the closure of the catalytic cycle; propylene can now attack the hydroperoxy species again, and the cycle can continue. However, we want to reiterate that in the final hydroperoxy intermediate (R) formed after the rotation of the geometry P, the H atom (no. 4) ends up being on the Au atom (no. 3), which was the (spectator) central Au atom of the obtuse angle Au_3 species in the main cycle. Also the OOH group ends up bonding on the Au atom (no. 1), which in the original hydroperoxy intermediate (geometry D, formed at the beginning of the cycle) hosted only an H atom.

In short, although the geometries R and D are exactly the same, they differ in the placement of the OOH and H (geometry R and D are position isomers). Therefore, this second subpathway may not lead to the (formal) closure of the cycle, if one or more of the Au atoms are strongly interacting with the support in the real catalyst. However, if the Au species are not very strongly anchored to the support and have reasonable freedom to rotate and move, then this second subpathway too could be an important part of the propylene epoxidation chemistry.

3.4. Alternative Entrance Channel Reactions. So far we only discussed the propylene epoxidation pathways starting from H−Au_3−OOH intermediate. We devote this subsection to highlight the importance of this choice by considering alternative entrance channel reactions.

As already stated in the Introduction, using INS studies, Goodman and co-workers[21] provide a strong evidence for the formation of OOH intermediates due to the reaction of H_2 and O_2 on Au/TiO_2 catalyst. This is the most important reason for our choice of hydroperoxy intermediate in the propylene epoxidation pathways reported above. Of course, scattering studies do not specifically tell us the existence of Au_3. However, Au_3 is our choice to model the chemistry. To support our choice of H−Au_3−OOH further, we performed additional calculations to examine pathways starting from O−Au_3−O (which may form due to O−O dissociation) and HO−Au_3−OH (which may form from H_2 and O_2 or due to decomposition of H_2O_2).

We note that the activation energy for O_2 dissociation on Au_3 is greater than 50 kcal/mol, i.e., substantially higher than that of the RDS in the pathway based on H−Au_3−OOH. Therefore, although it would be interesting to study interaction of propylene with O−Au_3−O, we rule out this particular pathway on Au_3 due to a very high activation barrier for the formation of O−Au_3−O. We also considered the decomposition of H−Au_3−OOH intermediate to water adsorbed on Au_3−O. This step has an activation barrier of about 19.3 kcal/mol. However, the ΔG (Gibbs free energy of products − Gibbs free energy of reactants) for this step is + 12.3 kcal/mol indicating a thermodynamically unfavorable formation of Au_3−O intermediate. Therefore, we rule out propylene epoxidation channels involving O−Au_3−O or Au_3−O intermediates.

In the case of HO−Au_3−OH, our calculations indicate that the O atoms have almost −1.00 NBO charge on them. This means that these O atoms are much less electrophilic than the proximal O atom (NBO charge −0.20) in the H−Au_3−OOH

intermediate. Since the epoxidation step involves electrophilic attack of O atom on the C═C of propylene, we believe that the activation barrier for the epoxidation step on HO−Au_3−OH could be much higher than that on H−Au_3−OOH.

All the aforementioned factors highlight the importance of considering H−Au_3−OOH intermediate over O−Au_3−O or HO−Au_3−OH to develop a propylene epoxidation scheme. We now discuss the implications of our propylene epoxidation pathway (involving H−Au_3−OOH intermediate) in the context of experimental and theoretical understanding of the epoxidaion system.

4. Discussion

There are several other ab initio "olefin epoxidation" studies (involving Ti sites but no Au), which report the activation barriers comparable to the activation barriers reported in this paper. We consider a few representative studies here. Vayssilov and van Santen[54] modeled the *ethylene* epoxidation at the Ti site of the TS-1 using the nondissociatively adsorbed hydrogen peroxide. They found the activation barrier for the epoxidation to be 19.9 kcal/mol (83.0 kJ/mol). Sinclair and Catlow,[55] for the same system, found the activation barrier for the ethylene epoxidation to be around 16.7 kcal/mol (70.0 kJ/mol) depending on the route followed. Munakata et al.[56] reported an activation barrier of 18.4 kcal/mol (77.0 kJ/mol) for the ethylene epoxidation at the hydrated Ti site of the TS-1. Wells et al.[53] studied the propylene epoxidation at the defect Ti site (T-6) in the TS-1. They found an activation barrier of the RDS to be 15.4 kcal/mol.

These studies all vary, not only in the chemistry of the olefin oxidation but also in the DFT method and cluster model of the Ti site. It is interesting to note that while all the aforementioned authors studied the epoxidation mechanisms on the active Ti site (no Au involved), we report an epoxidation mechanism on the Au_3 (without a Ti site involved), where the activation barrier (ΔE_{act}) of the *apparent* RDS (22.6 kcal/mol in the cycle with sub-pathway 2) for the propylene epoxidation is somewhat higher than that reported in the other studies (15−20 kcal/mol). We point out that based only on the electronic activation energy calculated at 0 K in a vacuum (ΔE_{act}) it appears that the water formation step in the subpathway 2 (or subpathway 1) is the RDS. However, the pre-exponential factor of this step is $\sim 10^4$ times higher than that of actual epoxidation step, i.e., propylene attack on the hydroperoxy intermediate. This is reflected by a higher ΔG_{act} of the actual epoxidation step than that of the water formation step in the subpathway 2 (and also in the subpathway 1). A quick calculation shows that, at 298 K, the rate constant (evaluated using the activation energy corrected with zero-point energy) for the water formation step in the subpathway 2 is actually 20 times larger than that calculated for the actual propylene epoxidation step. This means that the actual propylene epoxidation step is the true RDS in our pathways. In fact, one should always consider ΔG_{act} to determine the RDS, as it accounts for the contribution from both the activation energy and the pre-exponential factor. The latter is not considered if only ΔE_{act} is used to determine the RDS.

Unfortunately, the aforementioned olefin epoxidation studies involving Ti sites do not report the ΔG_{act} values. Therefore, we compare the activation energy (ΔE_{act}) of the actual epoxidation step in our Au-only pathway with aforementioned olefin epoxidation pathways involving Ti sites. In fact, the activation barrier (19.6 kcal/mol) of the actual epoxidation step in our Au-only mechanism is similar to the barriers reported in the aforementioned studies (15−20 kcal/mol). A possible implication is that epoxidation pathways on the Au as well as on the Ti site may coexist. This also means that there is a potential dual role played by the Au clusters: (i) generation of the oxidizing agent from H_2 and O_2, which then activates the Ti site, and (ii) propylene epoxidation. In the presence of the Ti, in addition to the epoxidation at the Ti center, Ti may promote the epoxidation activity by reducing the activation barriers in our pathway on the Au clusters located in its vicinity. These Au−Ti interactions could include charging of the Au cluster and Au cluster geometry distortion. More work is needed to explore these possibilities.

In this context, it is interesting to note that the recent experimental work[57] from our group shows that the high Si/Ti TS-1 materials show a positive correlation between the Ti loading and the Au loading. This suggests that the Au clusters have a tendency to anchor in the vicinity of the Ti sites in the TS-1. We have recently confirmed this finding with embedded cluster (QM/MM) calculations of adsorption of small Au clusters inside the TS-1 channels.[58] We found a stronger adsorption of the Au clusters near the Ti site of the TS-1, than that near the Si site in the S-1 lattice.[58]

In this study, we have used Au_3 as a model to demonstrate the epoxidation chemistry involving only Au. Since the catalytic activity of the Au clusters is known to vary with cluster size, it will be necessary to investigate the effect of Au cluster size as well as support interaction on the activation barriers in the proposed reaction pathway. An interesting implication of the findings on gas-phase Au_3 is that an epoxidation pathway involving only Au may remain valid for Au clusters deposited on any support and not just Ti-containing supports. We acknowledge that, under the typical experimental conditions, some other mechanism with lower activation barriers may prevail, but we believe that our Au-only pathway may offer a competitive channel for propylene epoxidation and hence merits consideration.

5. Conclusions

We have discovered a novel gas-phase propylene epoxidation mechanism on the neutral Au_3 using H_2 and O_2, which comprises two closely related pathways differing in the way the catalytic cycle undergoes closure. In the beginning of the cycle, the O_2 adsorbed on Au_3 facilitates the dissociative adsorption of H_2 to form a OOH intermediate, which remains adsorbed on the Au_3. The activation barrier for this step is only 2.2 kcal/mol. In agreement with experiments by Naito and Tanimoto[59] on Au/SiO_2, our calculations indeed predict an O_2-enhanced H_2 dissociation, e.g., the activation barrier (ΔE_{act}) for H_2 dissociation on naked Au_3 is $\sim$16 kcal/mol, while it reduces to $\sim$2 kcal/mol upon interaction of H_2 with the Au_3O_2 species (first H_2 addition step in our pathway).

The O atom (of the OOH) proximal to the Au atom is more electrophilic and attacks the C═C of the propylene to form PO. It is interesting to note that this chemistry is analogous to that in the olefin epoxidation at Ti−OOH site where Neurock and Manzer[60] first found that more electrophilic O atom (proximal to the Ti site) attacks the double bond of olefin. The activation barrier for our propylene epoxidation step is 19.6 kcal/mol. Product PO, which interacts with the Au_3, requires about 11.5 kcal/mol to desorb. It is interesting that the residual OH group (coming from the OOH group) actually migrates to the other terminal Au atom, which already hosts one H atom (a product of dissociated H_2). The Au_3 cluster from this step onward forms an obtuse angle triangular geometry. The bonding between the Au and H atoms is such that the H atoms have hydridelike character.

After the PO desorption step, the two subpathways can lead to the water formation and subsequent closure of the catalytic cycle. In the first pathway, the OH and H (crowded on the same terminal Au atom) approach each other to form water. The relatively high activation barrier (26.5 kcal/mol) of this step is due to the fact that the H atom partially coordinating with both the terminal and central Au atom actually loses its coordination with the central Au atom in the transition state, thus leading to the destabilization of the transition state. Water desorption requires 9.9 kcal/mol and leads to the regeneration of the Au_3 cluster (closure of the cycle). An important aspect of this first subpathway is that, in most of the steps the important events occur only on the terminal Au atoms, i.e., the central Au atom is just a spectator.

In the second subpathway, however, this is not the case. H_2 dissociatively adds in the Au−OH bond to form the water and another Au−H linkage. Although, the activation barrier for this step (22.6 kcal/mol) is higher than that of the actual epoxidation step (19.6 kcal/mol), the pre-exponential factor for the later is $\sim 10^4$ times smaller. In fact, we demonstrate that ΔG_{act} should be used to determine the true RDS, as it accounts for both the activation energy and the pre-exponential factor. On the basis of ΔG_{act}, we conclude that the actual propylene epoxidation step is the true RDS in our pathways. Therefore, we use the ΔE_{act} for the epoxidation step (Au-only pathway) for comparison with the olefin epoxidation pathways involving Ti sites (no Au). We found that the water desorption is, in fact, a spontaneous process and leads to the formation of obtuse angle Au_3 with two hydridelike H atoms connected to it. A rotation step leads to the formation of the (almost equilateral triangle) symmetric Au_3. It is noteworthy that one of the H atoms is actually connected to the central (in the geometries with obtuse angle) Au atom, which was just a spectator in all the previous steps.

Addition of O_2 in to the Au−H bonds leads to the formation of a hydroperoxy intermediate, which rotates to form a conformational isomer of the intermediate formed previously in the main reaction step (closure of the cycle). Therefore, this second subpathway actually utilizes all three Au atoms and may be viable only when the supported Au cluster is free to rotate and has sufficient mobility on the support.

We used the NBO charge analysis to describe the reaction chemistry as well as the geometric features of the reaction intermediates. We have reported the thermochemistry and the pre-exponential factors for the important steps in the reaction mechanisms; hence a complete kinetic and thermodynamic picture is presented.

We want to highlight that the epoxidation activation barrier ($\Delta E_{act} = 19.6$ kcal/mol) in our mechanism on Au_3 is comparable to the barriers reported (15−20 kcal/mol) in several other olefin epoxidation mechanisms on Ti sites in the absence of Au. Therefore, we advance the possibility of the Au playing a larger role than the mere production of the oxidizing agent from the H_2 and O_2 by offering a competitive epoxidation channel to that occurring on Ti. In future work it will be necessary to study whether the proximity between the Au and Ti on the supported catalyst can actually lower the activation barriers of the epoxidation channels on the Ti or Au or both. The results reported in this paper also imply the possibility that Au clusters on non-Ti supports could produce PO from propylene, H_2, and O_2.

Note Added in the Proof

While this manuscript was under revision two relevant papers from other groups were published. We discuss the implications these recent results and their connection with our findings reported in this manuscript.

Nijhuis et al.[61] studied epoxidation of propylene over Au/TiO_2 catalysts using H_2 and O_2. We refer the reader to Table 2 in their paper in which they also talk about non-Ti supports such as SiO_2. In fact, we point out that, on the 1% Au/SiO_2 catalyst (at 473 K), they found about 2.5% propylene conversion and 21% selectivity toward PO formation. Although, this performance is poor compared to Au/Ti-based catalysts, this result supports our computational finding of a propylene epoxidation pathway occurring on Au.

Hutchings and co-workers[62] reported a pioneering study demonstrating selective oxidation of hydrocarbons using molecular O_2 (no H_2) over Bismuth-modified Au/Carbon catalyst suspended in organic solvents. They found it is necessary to add a small quantity of radical initiator such as H_2O_2 or *tert*-butyl hydroperoxide (TBHP). In the absence of Au and/or radical initiator, very poor yields of selective oxidation products such as epoxides, ketones, and aldehydes (of cyclohexene, for example) were obtained. These results imply that both Au and radicals generated from H_2O_2 (possibly OOH) or TBHP are required to obtain excellent yields of selective oxidation products using molecular O_2 as oxidant. Therefore, we speculate that the selective oxidation reactions occur on Au and that radicals such as OOH may have a role in these reactions. Finally, we point out that, although our results in this manuscript do not account for the solvent effects, we do have a propylene epoxidation pathway occurring on Au with a major role played by the OOH group.

Acknowledgment. This work was funded by the National Science Foundation through Grant CTS-0238989-CAREER (K.T.T.) and by the United States Department of Energy, Office of Basic Energy Sciences, through Grant DE-FG02-01ER-15107 (W.N.D.). Computational resources were obtained through a grant from the National Computational Science Alliance (AAB proposal ESC030001) and through the supercomputing resources at Purdue University. A.M.J. thanks Yogesh Joshi, Dr. Aditya Bhan, Lasitha Cumaranatunge, and Brad Taylor for their help.

References and Notes

(1) Haruta, M.; Yamada, N.; Kobayashi, T.; Iijima, S. *J. Catal.* **1989**, *115*, 301.
(2) Haruta, M.; Tsubota, S.; Kobayashi, T.; Kangeyama, H.; Genet, M. J.; Delmon, B. *J. Catal.* **1993**, *144*, 175.
(3) Hammer, B.; Nørskov, J. K. *Nature* **1995**, *376*, 238.
(4) Haruta, M. *Catal. Today* **1997**, *36*, 153.
(5) Haruta, M.; Date, M. *Appl. Catal. A* **2001**, *222*, 427.
(6) Guzman, J.; Gates, B. C. *J. Phys. Chem. B* **2002**, *106*, 7659.
(7) Stangland, E. E.; Stavens, K. B.; Andres, R. P.; Delgass, W. N. *J. Catal.* **2000**, *191*, 332.
(8) Stangland, E. E.; Taylor, B.; Andres, R. P.; Delgass, W. N. *J. Phys. Chem. B* **2005**, *109*, 2321.
(9) Uphade, B. S.; Yamada, Y.; Akita, T.; Nakamura, T.; Haruta, M. *Appl. Catal. A* **2001**, *215*, 137.
(10) Uphade, B. S.; Akita, T.; Nakamura, T.; Haruta, M. *J. Catal.* **2002**, *209*, 331.
(11) Nijhuis, T. A.; Huizinga, B. J.; Makkee, M.; Moulijn, J. A. *Ind. Eng. Chem. Res.* **1999**, *38*, 884.
(12) Nijhuis, T. A.; Visser, T.; Weckhuysen, B. M. *Angew. Chem., Int. Ed.* **2005**, *44*, 1115.
(13) Mavrikakis, M.; Stoltze, P.; Nørskov, J. K. *Catal. Lett.* **2000**, *64*, 101.
(14) Yap, N.; Andres, R. P.; Delgass, W. N. *J. Catal.* **2004**, *226*, 156.
(15) Lopez, N.; Nørskov, J. K. *Surf. Sci.* **2002**, *515*, 175.
(16) Sanchez, A.; Abbet, S.; Heiz, U.; Schneider, W. D.; Häkkinen, H.; Barnett, R. N.; Landman, U. *J. Phys. Chem. A* **1999**, *103*, 9573.
(17) Clerici, M. G.; Bellussi, G.; Romano, U. *J. Catal.* **1991**, *129*, 159.
(18) Thomas, J. M.; Sankar, G.; Klunduk, M. C.; Attfield, M. P.; Maschmeyer, T.; Johnson, B. F. G.; Bell, R. G. *J. Phys. Chem. B* **1999**, *103*, 8809.

(19) Thiele, G. F.; Roland, E. *J. Mol. Catal. A* **1997**, *117*, 351.
(20) Ajo, H. M.; Bondzie, V. A.; Campbell, C. T. *Catal. Lett.* **2002**, *78*, 359.
(21) Sivadinarayana, C.; Choudhary, T. V.; Daemen, L. L.; Eckert, J.; Goodman, D. W. *J. Am. Chem. Soc.* **2004**, *126*, 38.
(22) Davis, K. A.; Goodman, D. W. *J. Phys. Chem. B* **2000**, *104*, 8557.
(23) Remediakis, I. N.; Lopez, N.; Nørskov, J. K. *Angew. Chem., Int. Ed.* **2005**, *44*, 1824.
(24) Chrétien, S.; Gordon, M. S.; Metiu, H. *J. Chem. Phys.* **2004**, *121*, 3756.
(25) Chrétien, S.; Gordon, M. S.; Metiu, H. *J. Chem. Phys.* **2004**, *121*, 9925.
(26) Chrétien, S.; Gordon, M. S.; Metiu, H. *J. Chem. Phys.* **2004**, *121*, 9931.
(27) Wells, D. H.; Delgass, W. N.; Thomson, K. T. *J. Catal.* **2004**, *225*, 69.
(28) Frisch, M. J.; Trucks, G. W.; Schlegel, H. B.; Scuseria, G. E.; Robb, M. A.; Cheeseman, J. R.; Montgomery, J. A., Jr.; Vreven, T.; Kudin, K. N.; Burant, J. C.; Millam, J. M.; Iyengar, S. S.; Tomasi, J.; Barone, V.; Mennucci, B.; Cossi, M.; Scalmani, G.; Rega, N.; Petersson, G. A.; Nakatsuji, H.; Hada, M.; Ehara, M.; Toyota, K.; Fukuda, R.; Hasegawa, J.; Ishida, M.; Nakajima, T.; Honda, Y.; Kitao, O.; Nakai, H.; Klene, M.; Li, X.; Knox, J. E.; Hratchian, H. P.; Cross, J. B.; Adamo, C.; Jaramillo, J.; Gomperts, R.; Stratmann, R. E.; Yazyev, O.; Austin, A. J.; Cammi, R.; Pomelli, C.; Ochterski, J. W.; Ayala, P. Y.; Morokuma, K.; Voth, G. A.; Salvador, P.; Dannenberg, J. J.; Zakrzewski, V. G.; Dapprich, S.; Daniels, A. D.; Strain, M. C.; Farkas, O.; Malick, D. K.; Rabuck, A. D.; Raghavachari, K.; Foresman, J. B.; Ortiz, J. V.; Cui, Q.; Baboul, A. G.; Clifford, S.; Cioslowski, J.; Stefanov, B. B.; Liu, G.; Liashenko, A.; Piskorz, P.; Komaromi, I.; Martin, R. L.; Fox, D. J.; Keith, T.; Al-Laham, M. A.; Peng, C. Y.; Nanayakkara, A.; Challacombe, M.; Gill, P. M. W.; Johnson, B.; Chen, W.; Wong, M. W.; Gonzalez, C.; Pople, J. A.; *Gaussian 03*, revision A.1; Gaussian, Inc.: Pittsburgh, PA, 2003.
(29) Becke, A. D. *J. Chem. Phys.* **1993**, *98*, 5648.
(30) Lee, C.; Yang, W.; Parr, R. G. *Phys. Rev. B* **1988**, *37*, 785.
(31) Vosko, S. H.; Wilk, L.; Nusair, M. *Can. J. Phys.* **1980**, *58*, 1200.
(32) Hay, P. J.; Wadt, W. R. *J. Chem. Phys.* **1985**, *82*, 270.
(33) Hay, P. J.; Wadt, W. R. *J. Chem. Phys.* **1985**, *82*, 299.
(34) Bond, G. C.; Thompson, D. T. *Catal. Rev.* **1999**, *41*, 319.
(35) Wesendrup, R.; Hunt, T.; Schwerdtfeger, P. *J. Chem. Phys.* **2000**, *112*, 9356.
(36) Pyykkö, P. *Angew. Chem., Int. Ed.* **2004**, *43*, 4412.
(37) Taylor, K. J.; Pettiette-Hall, C. L.; Cheshnovsky, O.; Smalley, R. E. *J. Chem. Phys.* **1992**, *96*, 3319.
(38) Moore, C. E. *Atomic Energy Levels*, Circ. No. 467; National Bureau of Standards: Washington, DC, 1958, Vol. III.
(39) Cheeseman, M. A.; Eyler, J. R. *J. Phys. Chem.* **1992**, *96*, 1082.
(40) Jackslath, C.; Rabin, I.; W. Schulze, B. B. *Phys. Chem.* **1992**, *96*, 1200.
(41) Curtiss, L. A.; Redfern, P. C.; Raghavachari, K.; Pople, J. A. *J. Chem. Phys.* **1998**, *109*, 42.
(42) Feller, D.; Davidson, E. R. *J. Chem. Phys.* **1989**, *90*, 1024.
(43) Rienstra-Kiracofe, J. C.; Tschumper, G. S.; H. F. Schaefer, I.; Nandi, S.; Ellison, G. B. *Chem. Rev.* **2002**, *102*, 231.
(44) *CRC Handbook of Chemistry and Physics*, 55th ed.; CRC Press: Cleveland, OH, 1974.
(45) Selim, E. T. M. *Ind. J. Pure Appl. Phys.* **1980**, *18*, 31.
(46) McAlduff, E. J.; Houk, K. N. *Can. J. Chem.* **1977**, *55*, 318.
(47) Glendening, E. D.; Reed, A. E.; Carpenter, J. E.; Weinhold, F. *NBO, Version 3.1*; Gaussian Inc.: Pittsburgh, PA, 2001.
(48) Joshi, A. M.; Delgass, W. N.; Thomson, K. T. *J. Phys. Chem. B* **2005**, *109*, 22392.
(49) Bravo-Pérez, G.; Garzón, I. L.; Novaro, O. *THEOCHEM* **1999**, *493*, 225.
(50) Howard, J. A.; Sutcliffe, R.; Mile, B. *Surf. Sci.* **1985**, *156*, 214.
(51) Ding, X.; Li, Z.; Yang, J.; Hou, J. G.; Zhu, Q. *J. Chem. Phys.* **2004**, *120*, 9594.
(52) Mills, G.; Gordon, M. S.; Metiu, H. *Chem. Phys. Lett.* **2002**, *359*, 493.
(53) Wells, D. H.; Delgass, W. N.; Thomson, K. T. *J. Am. Chem. Soc.* **2004**, *126*, 2956.
(54) Vayssilov, G. N.; van Santen, R. A. *J. Catal.* **1998**, *175*, 170.
(55) Sinclair, P. E.; Catlow, C. R. A. *J. Phys. Chem. B* **1999**, *103*, 1084.
(56) Munakata, H.; Oumi, Y.; Miyamoto, A. *J. Phys. Chem. B* **2001**, *105*, 3493.
(57) Taylor, B.; Lauterbach, J.; Delgass, W. N. *Appl. Catal. A* **2005**, *291*, 188.
(58) Joshi, A. M.; Delgass, W. N.; Thomson, K. T. In preparation, 2005.
(59) Naito, S.; Tanimoto, M. *J. Chem. Soc., Chem. Commun.* **1988**, *12*, 832.
(60) Neurock, M.; Manzer, L. E. *Chem. Commun.* **1996**, 1133.
(61) Nijhuis, T. A.; Visser, T.; Weckhuysen, B. M. *J. Phys. Chem. B.* **2005**, *109*, 19309.
(62) Hughes, M. D.; Xu, Y.-J.; Jenkins, P.; McMorn, P.; Landon, P.; Enache, D. I.; Carley, A. F.; Attard, G. A.; Hutchings, G. J.; King, F.; Stitt, E. H.; Johnston, P.; Griffin, K.; Kiely, C. J. *Nature* **2005**, *437*, 1132.